Patterns of geochemical variability across weakly developed paleosol profiles and their role as regional stratigraphic markers (Upper Pleistocene, Po Plain)

Published Version:
Amorosi A., Bruno L., Campo B., Di Martino A., Sammartino I. (2021). Patterns of geochemical variability across weakly developed paleosol profiles and their role as regional stratigraphic markers (Upper Pleistocene, Po Plain). PALAEOGEOGRAPHY PALAEOCLIMATOLOGY PALAEOECOLOGY, 574, 1-13 [10.1016/j.palaeo.2021.110413].

Availability:
This version is available at: https://hdl.handle.net/11585/871198 since: 2022-02-27

Published:
DOI: http://doi.org/10.1016/j.palaeo.2021.110413

Patterns of geochemical variability across weakly developed paleosol profiles and their role as regional stratigraphic markers (Upper Pleistocene, Po Plain)

Alessandro Amorosi[1*], Luigi Bruno[2], Bruno Campo[1], Andrea Di Martino[1], Irene Sammartino[3]

[1]Department of Biological, Geological and Environmental Sciences, University of Bologna, Italy.
E-mail: alessandro.amorosi@unibo.it, bruno.campo@unibo.it, andrea.dimartino4@unibo.it
[2]Department of Chemical and Geological Sciences, University of Modena and Reggio Emilia, Italy.
E-mail: luigi.bruno@unimore.it
[3]Geologic consultant, Bologna, Italy. E-mail: Irene.sammartino@gmail.com
*Corresponding author

Abstract

Weakly developed paleosols from two distinct interfluve surfaces of Late Pleistocene age provide excellent keys to high-resolution stratigraphic correlation and may serve to trace large-scale genetic packages (systems tract equivalents) across the continental portion of the Po Basin. Twenty-four paleosol profiles from 17 sediment cores were identified and characterized for bulk-geochemical analysis. X-ray fluorescence data were used to trace the degree of weathering. Paleosols, 0.5-1.5 m thick, are pedogenically altered floodplain deposits, developed over time spans of a few thousand of years and mostly partitioned into A-Bk horizons. The most notable paleosol features are dark, organic-matter-rich and carbonate-free mineral surface horizons (A) that overlie bright calcic horizons (Bk) typified by the accumulation of secondary carbonates in the form of pedogenic nodules.

Paleosol profiles exhibit a homogeneous geochemical signature that fingerprints a moderate degree of weathering, with little strike- and dip-oriented variability across the different study localities. Plots of Al-normalized calcification and base loss indices against depth reveal systematic increasing values from intensely altered A horizons to underlying Bk horizons. These trends reflect consistent patterns of Ca translocation from surface horizons deeper into the profile, with significant to almost complete Ca removal from A horizons through leaching and accumulation in Bk horizons. Selected trace element ratios (Ba/Sr, Rb/Sr), redox-sensitive trace elements and Zr contents display opposite, up-profile increasing trends that reflect Sr loss in A horizons, with selective Zr concentration in residual minerals.

Vertical trends in element ratios are laterally extensive and consistent on a regional basis and represent key pedochemical/stratigraphic markers that can be traced over great distances (tens of

kms) throughout the inland portion of the basin. Through quantitative assessment of the degree of weathering, geochemical profiling provides high potential for robust subsurface paleosol correlation that might not be captured by visual core descriptions alone.

Keywords: Paleosol stratigraphy; Paleosol maturity; Interfluve; Sequence stratigraphy; Sequence boundary; Geochemistry

1. Introduction

Paleosol-bearing alluvial successions contain a hierarchical record of cyclic sediment accumulation produced in response to the combined effect of autogenic and allogenic controlling mechanisms (Cleveland et al., 2007). Paleosols at sequence-bounding unconformities, in particular, may serve as useful regional stratigraphic markers to trace genetic packages across the basin and to determine regional accommodation trends (Demko et al., 2004).

According to sequence-stratigraphic models, paleosol units commonly correlate with incision along the major drainage axes (Van Wagoner et al., 1990) and well-developed, mature interfluve paleosols correlate to valley-floor erosion surfaces (Gibling and Bird, 1994; Aitken and Flint, 1996; Shanley and McCabe, 1994; McCarthy and Plint, 1998; 2003; Plint et al., 2001; Atchley et al., 2004; Blum and Aslan, 2006; Cleveland et al., 2007; Srivastava et al., 2010; Raigemborn and Beilinson, 2020).

Models of paleovalley architecture and paleosol-valley relations have been evaluated using Quaternary examples, where proxy records are well established for climate and sea level and periods of incision and aggradation can generate discontinuity-bounded sequences on timescales as short as 10^3 to 10^4 years (Gibling et al., 2011). In such examples, valley fills are less distinctive and their bases do not correspond to prominent paleosols. Stacked weakly developed paleosols may form terrestrial condensed sections that record prolonged periods of minimal sedimentation in interfluve position (Gibling et al., 2011; McCarthy and Plint, 2013).

Vertical successions of poorly mature paleosols have been widely described from the Upper Pleistocene subsurface record of the Po Plain, in Italy (Amorosi et al., 2017b; Bruno et al., 2018). Stiff, pedogenized floodplain silts and clays are widely preserved south of the modern Po River and correlate in the north to genetically-related fluvial facies, where thick channel-belt sand bodies represent the dominant subsurface stratigraphic unit (Fig. 1).

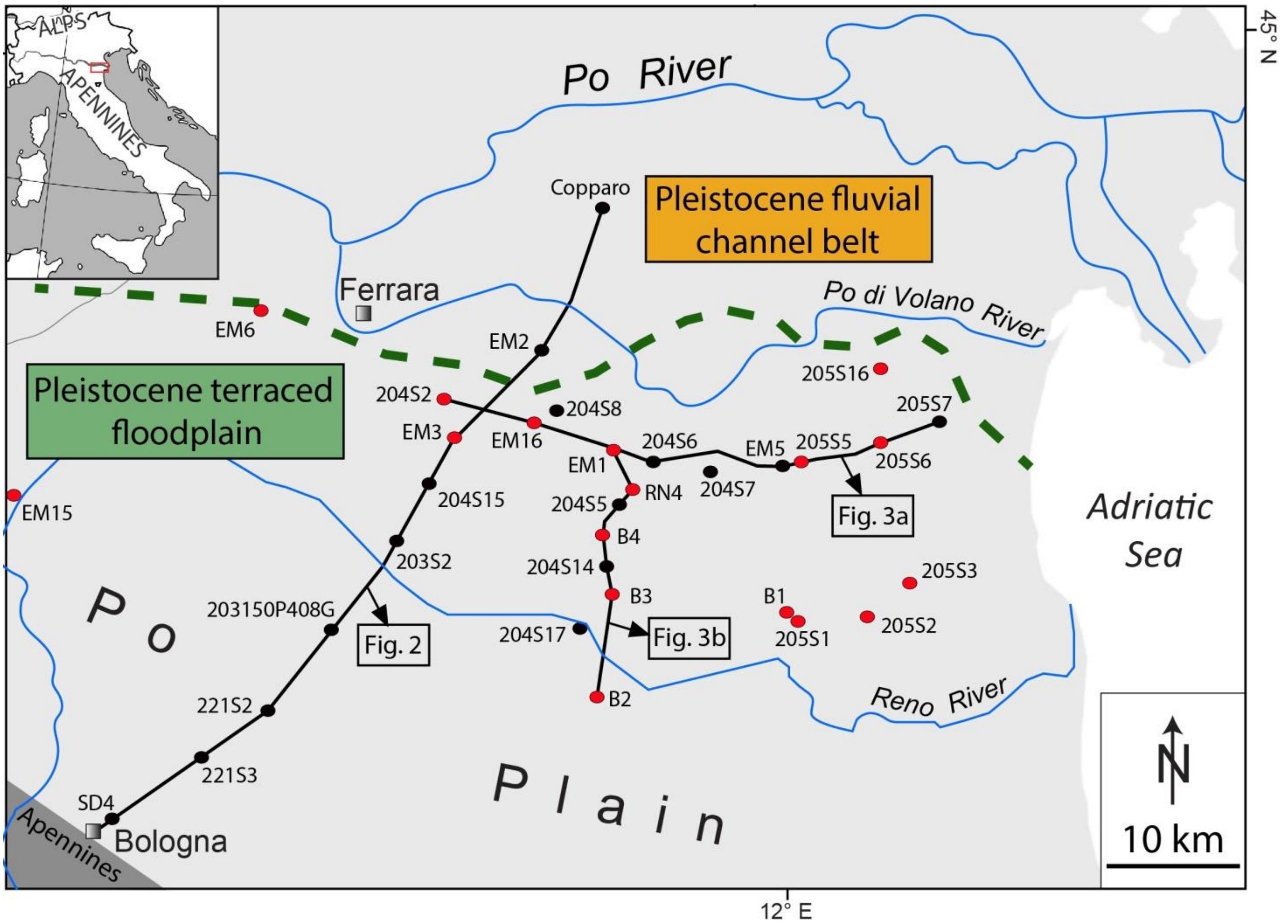

Fig. 1. Location map of studied cores (red dots), with indication of the boundary between the buried Pleistocene (pre-LGM) terraced floodplain and the coeval fluvial channel-belt sand bodies (green dashed line, from Morelli et al., 2017). Section trace of Figure 2, transects in Fig. 3, and location of additional cores used for stratigraphic correlation (black dots) are also shown.

The Upper Pleistocene-Holocene sedimentary succession provides a particularly well-established temporal framework, founded largely on ^{14}C data, within which immature paleosols delineate time-equivalent stratal surfaces and represent key stratigraphic markers that can be traced on a regional scale. Three paleosols of Late Pleistocene age (P1-P3) and a younger paleosol marking the Pleistocene-Holocene boundary (PH) were recognized for the first time from core analysis in the Bologna area (Amorosi et al., 2014a). Subsequent studies examined the basin-scale distribution of these paleosols (Amorosi et al., 2017b; Bruno et al., 2019) and their likely climatic significance (Bruno et al., 2020). Morelli et al. (2017) carried out the detailed subsurface mapping of the youngest two paleosols: paleosol P3, formed at the onset of the Last Glacial Maximum

(LGM), and paleosol PH, encompassing the Younger Dryas (YD) cold event, which marked the short-lived return to glacial conditions after the Late Glacial Interstadial. Although upper Quaternary paleosols clearly exhibit a high potential for regional correlations, only reconnaissance geologic investigation has been undertaken and no detailed paleosol characterization has been attempted, so far.

In this study, a comprehensive geochemical investigation of paleosols P3 (LGM paleosol) and PH (YD paleosol) was performed for the first time. The aim of this paper is to provide quantitative assessment of paleosol maturity across these two pedogenized key stratigraphic surfaces, which in a sequence-stratigraphic perspective coincide with the sequence boundary (SB) and the landward equivalent of the transgressive surface (TS), respectively (Fig. 2). Specific objective is to document the stratigraphic utility of immature paleosols for regional correlations within a chronologically constrained sequence-stratigraphic framework. Below the Holocene succession, the study area reveals a wide, buried Late Pleistocene interfluve between the Apennines margin and the coeval fluvial channel-belt bodies in the modern Po River area (Fig. 1). Age-equivalent strata successions are compared from 17 sediment cores, approximately 80 km apart. This study incorporates high-resolution stratigraphic data, paleosol descriptions and geochemistry.

2. Stratigraphic overview

Previous work provides a solid foundation of the shallow subsurface stratigraphy of late Quaternary continental deposits in the Po Plain (Amorosi et al., 2014a; 2017b; Morelli et al., 2017; Bruno et al., 2018; 2020). In this rapidly subsiding setting with high rates of sedimentation, no persistent incised valley was established during the last interglacial/glacial transition and aggradationally-stacked, shallow-incised fluvial bodies are laterally associated with overbank packages, a few m thick, bounded by poorly mature paleosols (Amorosi et al., 2017b – Fig. 2). These paleosols, which define large-scale, though shallow degradation across the Po Plain interfluve, associated to short (2-5 kyr) gaps in sedimentation document widespread, but short-lived, subaerial weathering across poorly dissected, interfluvial areas (Amorosi et al., 2017b; Bruno et al., 2020).

A hierarchy of Upper Pleistocene paleosols has been identified and framed through high-resolution sequence stratigraphic analysis within a strongly constrained chronological setting, founded on tens of radiocarbon dates (Fig. 2). Two prominent paleosols, in particular, exhibit very high lateral continuity on a regional scale and are genetically related to fluvial channel-belt sand bodies identified to the north, beneath the modern Po River (Morelli et al., 2017 – Fig. 2). Paleosol-bounded overbank intervals have sequence-stratigraphic significance within the LGM depositional sequence and represent low-accommodation deposits. Based on detailed stratigraphic correlation with coeval littoral and shallow-marine facies associations, the two paleosols (paleosols P3 and PH of Amorosi et al., 2014) have been interpreted to represent the sequence boundary (SB) and the landward equivalent of the transgressive surface (TS), respectively (Amorosi et al., 2017a – Fig. 2).

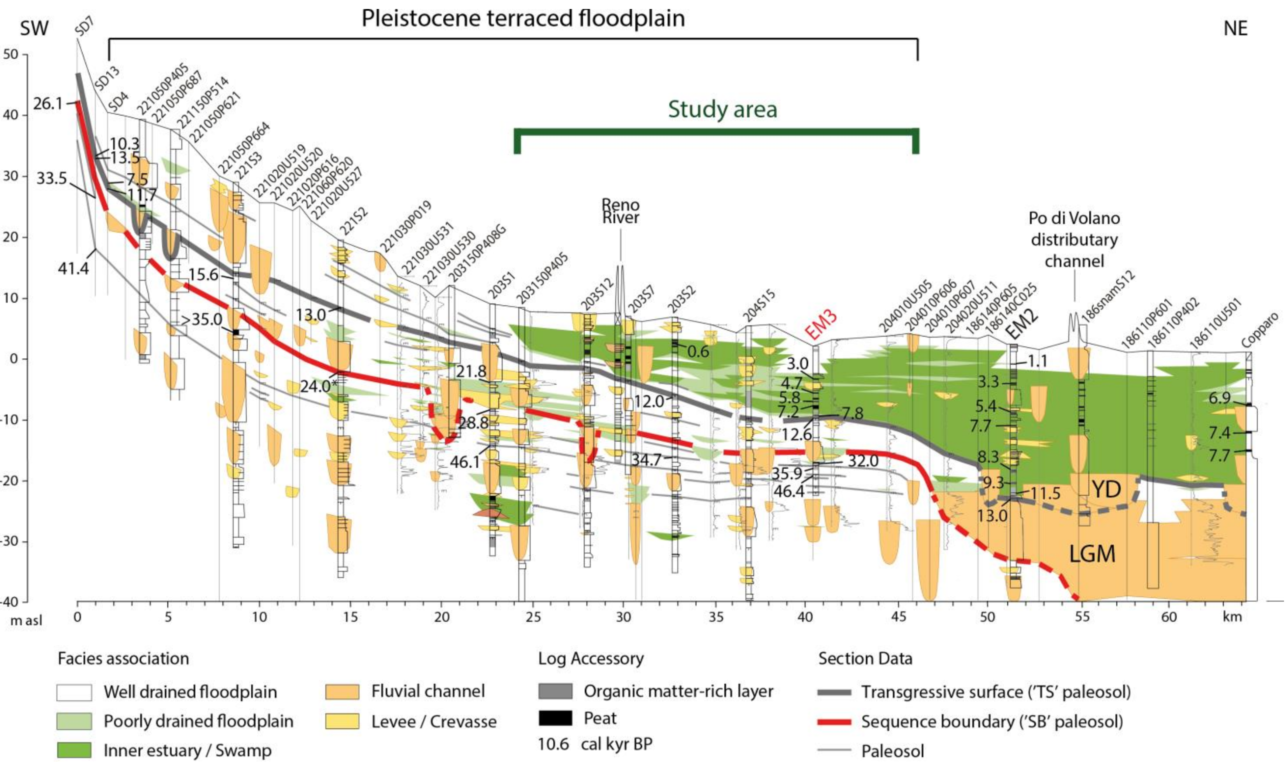

Fig. 2. Regional stratigraphic cross-section (section trace in Fig. 1) showing relationship of floodplain paleosols to their contemporaneous fluvial channel-belt sand bodies (modified after Amorosi et al., 2017b). Weakly-developed paleosols are typically arranged in thin, paleosol-bounded overbank sequences and are associated to larger trunk channels amalgamated into multilateral channel belts. The paleosol at the sequence boundary ('SB' paleosol) was generated at the MIS 3/2 transition and correlates to fluvial channel-belt bodies assigned to the Last Glacial Maximum (LGM). The landward equivalent of the transgressive surface ('TS' paleosol) marks the Pleistocene-Holocene boundary and correlates to Younger Dryas (YD) channel belts.

Sea-level lowering and climate-driven forcing have been invoked to account for shallow incision and coeval soil development in the Po Plain during the latest Pleistocene (Amorosi et al., 2017b;

Bruno et al., 2018; 2020). Pedogenic modification of floodplain silts and clays occurred at the MIS (Marine Isotope Stage) 3/2 transition, between 30 and 24 cal kyr B.P. (SB paleosol), and during the protracted sea-level lowstand, when fluvial entrenchment terraced the formerly active (pre-LGM) alluvial plain, which underwent extensive pedogenic modification. Shallowly-incised tributary valleys (see Kvale and Archer, 2007) form part of a surficial (Cremaschi, 1987; Castiglioni, 2001; Bersezio et al., 2007) and subsurface (Bruno et al., 2017b, 2018; Morelli et al., 2017) mappable drainage network feeding into the much larger Po fluvial system.

The SB interfluve paleosol caps a series of weakly expressed profiles that reflect multiple-step pedogenic history mostly occurring during MIS 3 (Bruno et al., 2020). Individual paleosols are generally stacked and separated by thin layers of overbank material (compound paleosols of Marriott and Wright, 1993). However, they may locally display overlapping profiles with A-B overprinting (composite paleosols) and pedogenic features may extend throughout much of the stratigraphic section. The SB paleosol correlates to the base of highly lenticular, valley-filling sand bodies, typically 20 to 30 m thick and 5 to 20 km wide, that display virtually no pedogenesis (Fig. 2).

A younger, regionally extensive paleosol (TS paleosol in Fig. 2) correlates with a short-lived episode of shallow fluvial incision developed around the Pleistocene-Holocene boundary (Amorosi et al., 2017b). Radiocarbon dates from this paleosol in the study area cluster around the Younger Dryas cold reversal (Fig. 2). Paleosol TS is simple. In the subsurface of the modern coastal plain it is invariably overlain by a deepening-upward succession of Holocene swamp, lagoonal, coastal and shallow-marine deposits and for this reason it is interpreted as the landward equivalent of the TS.

Soil formation at the MIS 3/2 transition has been described from other parts of the world. The primary influence on regional water table lowering at the MIS 3/2 transition was relative sea-level fall (Blum and Price, 1998; Dabrio et al., 2000; Autin and Aslan, 2001; Anderson et al., 2004; Busschers et al., 2007; Kasse et al., 2010; Fan et al., 2018). Similar, coeval paleosols have been reported from the Yangtze River, where compound paleosols (pedocomplexes) resulted from alternating deposition and pedogenesis on the paleointerfluve (Chen et al., 2008). Fluvial incision and soil development around the Pleistocene/Holocene boundary have been recorded in other European fluvial systems (Mol et al., 1997; van Balen et al., 2010; Janssens et al., 2012).

3. Methods

Within detailed measured sections from 17 cores (Fig. 1, Supplementary Table 1), 24 soil profiles were investigated and characterized for geochemical composition. Ten paleosols marking the sequence boundary ('SB' paleosols) and 14 younger paleosols formed at the transgressive surface ('TS' paleosols) were studied. The locations of the cores were chosen to provide as extensive coverage as possible across the two terraced paleosurfaces (Morelli et al., 2017). Geochemical analysis was carried out on all the study cores to extract elemental concentrations. A total of 100 soil samples were analyzed (Supplementary Table 2): 62 from 'TS' paleosols and 38 from compound/composite 'SB' paleosols. We also analyzed 11 samples from unaltered floodplain parent material from the same cores. This study is based largely on the stratigraphic distribution of macromorphological features of pedogenesis and on geochemical characterization of paleosols. Micromorphological investigations were not attempted.

Cores, 17 to 52 m thick, were split lengthwise and carefully described for their sedimentological characteristics. Facies analysis was carried out on a centimetre scale. Graphic logs of cores include description of lithology, grain size, primary sedimentary structures, lamination styles, bioturbation levels and accessory components.

Paleosols at key stratigraphic intervals were recognized by visual inspection of core material. Profile descriptions include horizonation, horizon thickness, color, reaction, redoximorphic features, carbonate accumulations, and other standard soil observations. Moist colors of mottles and matrix were described. Composition, size, and abundance of nodules and other mineral segregations were also characterized. Geotechnical properties were obtained through pocket penetration measurements. Horizon designations are based upon core-observed features in the paleosols after Soil Taxonomy (Soil Survey Staff, 1999).

Paleosols were sampled by horizon for bulk chemical analysis. Series of three to six samples were taken per paleosol profile from the top to a maximum depth of 150 cm. Major and trace element geochemistry was determined by X-ray fluorescence spectroscopy (XRF). Cores were analyzed at Bologna laboratories. Samples were oven dried at 50°C, powdered and homogenized in an agate mortar and analyzed using a Philips PW 1480 spectrometer (Philips, Almelo, The Netherlands). The matrix correction methods of Franzini et al. (1972), Leoni and Saitta (1976) and Leoni et al. (1982) were followed.

Analytical methods resulted in data for 29 elements: 10 major elements, reported as oxide percent by weight (SiO_2, TiO_2, Al_2O_3, Fe_2O_3, MnO, MgO, CaO, Na_2O, K_2O, and P_2O_5), 18 trace elements (Ba, Ce, Co, Cr, Cu, Ga, La, Nb, Ni, Pb, Rb, S, Sc, Sr, V, Y, Zn, and Zr), and the loss on ignition (LOI). LOI, evaluated after overnight heating at 950°C (LOI_{950}), represents a measure of volatile substances (weight %, wt%), including pore water, inorganic carbon and organic matter. The XRF analytical protocol reports major elements in oxide weight percent and trace elements in parts per million. The estimated precision and accuracy for trace element determinations were better than 5%. For elements with low concentrations (<10 mg/kg), the accuracy was 10%.

4. Paleosol stratigraphy

The Upper Pleistocene-Holocene stratigraphy in the study area was depicted along two transects, on the basis of stratigraphic and sedimentological data from 18 continuous cores and 36 piezocone (CPTU) penetration tests (Fig. 3). The W-E transect (Fig. 3a) runs roughly in proximal to distal direction across the buried Pleistocene terraced floodplain, 5-15 km from the southern margin of the Po paleovalley system, whereas the S-N transect (Fig. 3b) runs perpendicular to the regional axis of the Northern Apennines (Fig. 1).

In this study, we did not focus on facies architecture, which has been the subject of several published papers and that will not be reiterated here. Summary characteristics of major facies associations are summarized in Table 1. For detailed description and interpretation of coastal plain to shallow-marine deposits, the reader is referred to previously published material (Amorosi et al., 2017a; 2020; Bruno et al., 2017b; 2019; Campo et al., 2020). In this paper, we focused, instead, on the identification, characterization and tracing of paleosols at two discrete stratigraphic horizons, corresponding to the SB and TS (Fig. 2). Paleosols identified in cores (Fig. 4) were calibrated against CPTU tests and tracked laterally based on distinctive changes in log character. The key geotechnical features to infer paleosols from CPTU tests include: (i) a subtle, but consistent increase in cone resistance with depth, (ii) a sharp peak in the sleeve friction, recording the sharp contrast between normally consolidated floodplain facies and underlying stiff, pedogenically modified deposits, and (iii) an abrupt decrease in pore pressure (Amorosi and Marchi, 1999; Choi and Kim, 2006; Amorosi et al., 2017b; Bruno et al., 2019).

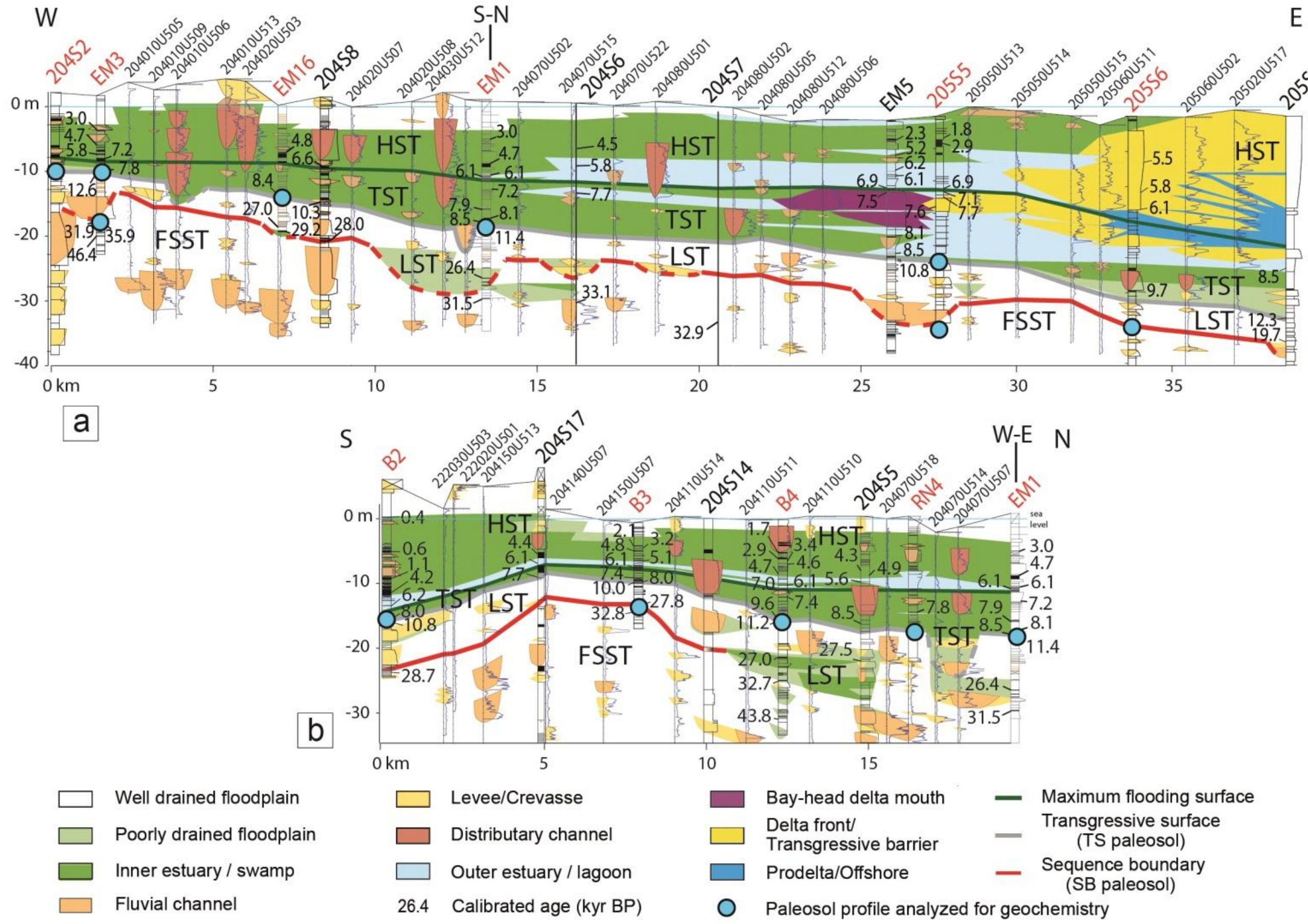

Fig. 3. Sequence stratigraphy of Upper Pleistocene-Holocene deposits from the subsurface of the Po Plain, with position and correlation of 'SB' (red line) and 'TS' (grey line) paleosols. Cores analyzed in this paper are marked in red. Radiocarbon dates from Amorosi et al. (2017a) (upper transect) and Amorosi et al. (2020) (lower transect). FSST: Falling-stage systems tract, LST: Lowstand systems tract, TST: transgressive systems tract, HST: highstand systems tract.

In the study area, the SB paleosol bears radiometric dates in the age range of 29.2-27.8 cal kyr B.P. (Fig. 3). It is underlain by a set of closely-spaced paleosols that exhibit slightly older ages (Fig. 3). Regional stratigraphy above this paleosol includes a thin (4-7 m) lowstand systems tract capped by the TS paleosol, with age ranges between 12.6 and 11.2 cal kyr B.P. (Fig. 3). The TS paleosol marks a regional facies change above Pleistocene alluvial deposits and it is overlain by a basinally mappable transgressive surface (TS in Fig. 3).

Facies Association	Lithology Sedimentary structures	Fossils
Fluvial channel	coarse to medium sand, FU trend, high-angle cross-lamination, 2-10 m thick	generally barren
Crevasse/levee	alternating sand and silt,parallel lamination, climbing ripples, 0.5-3 m thick	
Floodplain	clay and silty clay, bioturbation, root traces, mottling, paleosols, 1-20 m thick	generally barren, rare freshwater
Poorly drained floodplain	organic-matter-rich clay, roots, plant remains, 1-5 m thick	rare freshwater
Distributary channel	medium to fine sand, FU trend, high-angle cross-lamination, 2-10 m thick	generally barren, rare freshwater to low brackish
Bay-head delta	medium to fine sand, high-angle cross-lamination, plant debris, 2-5 m thick	mixed freshwater/brackish
Inner estuary/swamp	soft clay, plant debris, wood fragments, peat, parallel lamination, 1-20 m thick	freshwater to low brackish
Outer estuary/lagoon	bioturbated clay, clay-sand alternations, 1-5 m thick	brackish
Delta front/beach barrier	fine to coarse sand, high-angle cross-lamination, parallel lamination, 1-10 m thick	littoral
Prodelta/offshore	organic-matter-rich silty clay, bioturbated clay, 1-7 m thick	marine

Table 1. Summary characteristics of major lithofacies assemblages in the study area.

The Holocene succession displays a characteristic retrogradational to aggradational/progradational stacking pattern of facies that defines the transgressive systems tract (TST) and highstand systems tract (HST), respectively (Fig. 3). Holocene deposits rest unconformably on the TS paleosol with typical onlap geometries (Fig. 3a) and provide a detailed understanding of the stratigraphic development of the coastal plain under transgressive and normal regressive conditions. They cover a great diversity of facies associations (Campo et al., 2017) that represent coeval depositional environments, ranging from shallow-marine (offshore and prodelta) through coastal, brackish (outer estuary/lagoon) and freshwater (inner estuary/low-lying swamps).

In the study area, the top surface of the TS paleosol coincides with the landward equivalent of a surface of marine flooding that denotes subsequent transgression (Fig. 3a). Over most of the study area, the overlying Holocene sedimentary succession is dominated by single-story distributary-channel sand bodies encased in organic-rich clays, with a tongue of thin brackish (lagoonal) deposits that demarcate the maximum flooding surface (Fig. 3b). Peat-bearing deposits accumulated in low-lying, permanently waterlogged environments in the inner portion of a transgressive estuary and in the delta plain of a prograding delta system.

There is no dramatic change in depositional style in the two sections of Fig. 3, except for the notable deformation of Quaternary strata in the 204S17-B3 cores area (Fig. 3b), which has been interpreted to reflect recent tectonic activity of the buried anticline structures (Amorosi et al., 2020). Though discontinuous due to local truncation or poor development onto sandy substrates, paleosols on floodplain deposits can be typically traced laterally for about 40 km and appear to have been developed on a gently inclined slope (Fig. 3).

5. Paleosol description

Upper Pleistocene paleosols in the subsurface of the Po Plain are easily differentiated from overlying and underlying (unaltered) units by their stiff texture and color-banded appearance (Fig. 4). They all are silt- and clay-rich and are typically formed on muddy (floodplain) deposits.

Soil profiles typically consist of a dark, organic-rich and bioturbated silt (A horizon) that gradually overlies a paler horizon (Bk). Paleosol colors are relatively uniform throughout horizons A and B. Dominant colors are grey to brownish grey and dark brown in horizons A and light grey to pale yellow in the deeper horizons (Fig. 4).

Organic matter imparts the dark color in A horizons. Macroscopic features include root traces, wood debris, and plant fragments that are scattered throughout the unit. A horizons are barren with fossils and weakly reactive or unreactive to 10% dilute HCl. Pedogenic carbonate appears within 30-80 cm of the soil surface (Bk horizon), persisting to depths of about 100-150 cm (Fig. 4). Calcic horizons (Soil Survey Staff, 1999) can be thick and diffuse or thinner and more concentrated. Within Bk horizons, $CaCO_3$ concretions are visible to the naked eye, generally as pseudomycelia and few to common hard nodules. Powdery and filamentous carbonate is commonly observed between nodules. Carbonate nodules are well-rounded to sub-rounded and range from diffuse, poorly cemented concentrations to discrete, well-cemented masses. Locally, nodules may be larger than > 1 cm in diameter and may coalesce to form cemented or indurated, thin massive layers (Bkm).

A less common subsurface paleosol horizon that may be associated to the Bk horizon is Bw (Fig. 4). Pedogenized deposits in this case display root traces, local yellow, brown and orange colors and no carbonates. Black mottles likely derive from different manganese oxide species coating primary particles.

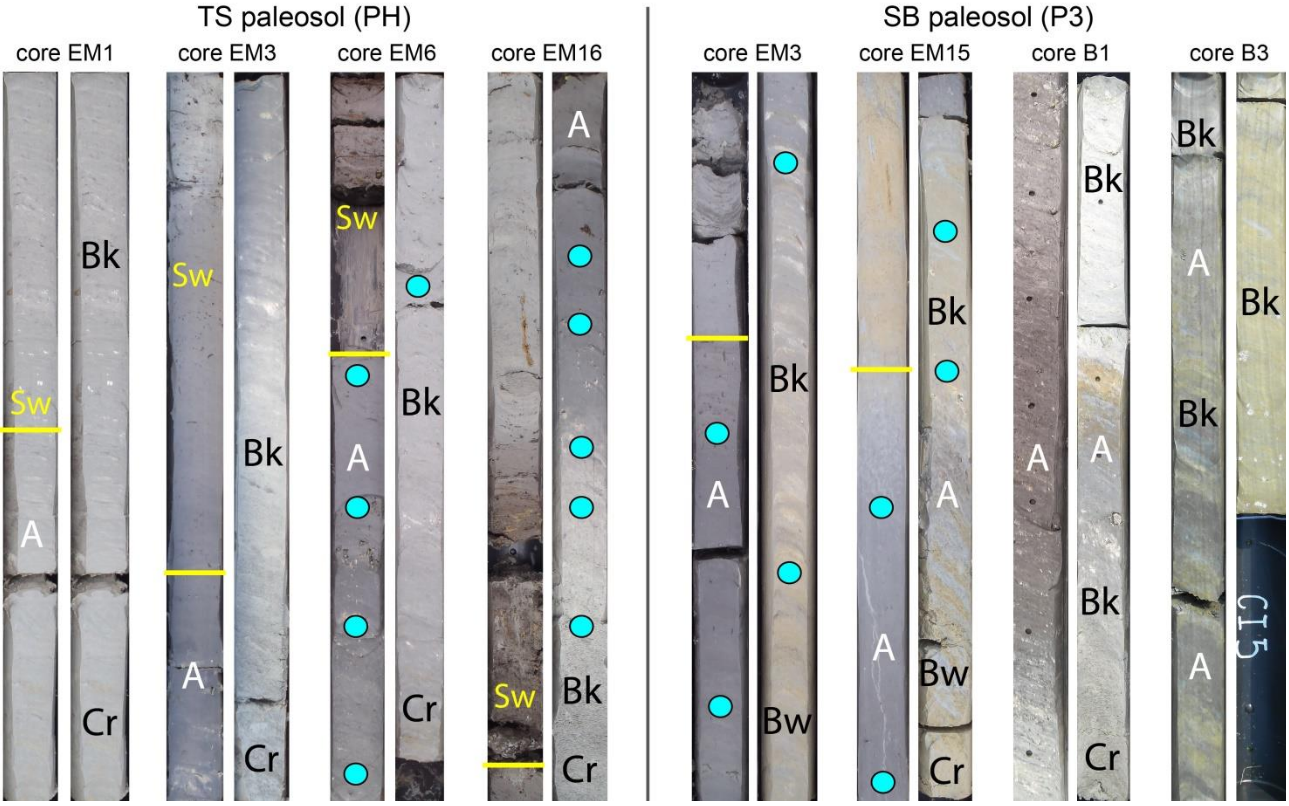

Fig. 4. Representative profiles of paleosols 'TS' and 'SB' showing A/Bk/Bw/Cr horizonation (for location, see Fig. 1; paleosol stratigraphy in Fig. 3). TS paleosols are simple A/Bk profiles, invariably overlain by Holocene transgressive deposits (inner estuary/swamp facies association - Sw), suggesting increased waterlogging and flooding in response to a rising water table. Paleosols spanning the sequence boundary (SB) consist of vertically stacked immature paleosols. Light blue dots indicate samples plotted in the geochemical profiles of Fig. 6. Core length is 1 m.

The unweathered (Cr) horizon retains the character of the unconsolidated parent material (floodplain deposits) and as such does not display pedogenic structure or significant rooting. To define the original material, we also determined average bulk compositions of unweathered floodplain sedimentary packages from the same stratigraphic succession.

Paleosols identified in cores also exhibit diagnostic engineering properties (Amorosi et al., 2015), with substantially higher compressive strength coefficients than all other fine-grained, alluvial (floodplain) facies. Specifically, paleosols are typified by distinctive penetration resistance, in the range of 3.5-5 kg/cm^2, with maximum values in Bk horizons (Amorosi et al., 2015). On the other hand, non-pedogenized floodplain deposits invariably display lower pocket penetration values (average value: 2.0 kg/cm^2).

6. Paleosol geochemistry

Major elements are commonly used to define the net effect of ancient chemical weathering from paleosols (Retallack, 2001). Several oxide ratios have been developed to assist with the interpretation of soil-forming processes in paleosols (Birkeland, 1999; Retallack, 2001). In general, alkali (Na and K) and alkaline earth (Ca and Mg) elements are mobile (Sheldon and Tabor, 2009) and are preferentially released from their host minerals during weathering (Mohanty and Nanda, 2016), whereas the elements Al, Ti and Zr are considered to be chemically immobile in weathering environments.

Several major element indices, such as the Chemical Index of Alteration-CIA, $Al_2O_3/(Al_2O_3+CaO+Na_2O+K_2O)$ (Nesbitt and Young, 1982), the Chemical Weathering Index-CWI, $Al_2O_3/(Al_2O_3+CaO+Na_2O)$ (Harnois, 1988), or the ∑Bases/Al ratio, $(CaO+MgO+Na_2O+K_2O)/Al_2O_3$ (Retallack, 1999) provide an indication of leaching of the bases from the soil system in response to weathering intensity, measuring the loss of mobile cations Ca^{2+}, Mg^{2+}, Na^+ and K^+, given as oxides, with respect to stable alumina (Ruxton, 1968; Retallack, 1999; Sheldon and Tabor, 2009). These indices, based on the ratio of a group of highly mobile oxides to one or more immobile oxides, are the best candidates to characterize weathering-induced changes (Price and Velbel, 2003; Varela et al., 2018).

In order to compensate for textural heterogeneity, in general we used elemental ratios over simple single-element measurements (Sheldon and Tabor, 2009). To facilitate interpretation of changes in geochemical composition as a result of soil development, values were also calculated from the unweathered parent material, corresponding to Pleistocene floodplain muds (Table 2).

Among the various chemical indices widely used to estimate weathering, we chose key indicators closely related to pedogenic processes (Retallack, 1997a,b,c; Driese et al., 2000; Sheldon and Tabor, 2009): SiO_2 for the framework material, Al_2O_3 for the clay component, CaO and Sr for the carbonate component, labile oxides for the degree of weathering, Zr for residual minerals. Owing to possible biases due to the overwhelming role of Ca relative to Na and K in the study samples (see values of labile oxides in Table 2), we did not use CIA and CWI as primary indicators of the degree of weathering. We also did not select element ratios that include iron in their formulation, because iron concentrations are a reflection of redox conditions, which may be controlled by modern or ancient groundwater levels and may not be consistent throughout the weathering profile (Harnois, 1988).

Horizon	Surface	SiO_2 (%)	±	TiO_2(%)	±	Al_2O_3(%)	±	Fe_2O_3(%)	±	MnO (%)	±	MgO (%)	±	CaO (%)	±	Na_2O (%)	±	K_2O (%)	±	P_2O_5 (%)	±
A	SB	56.50	5.10	0.75	0.08	16.48	1.54	5.72	1.03	0.05	0.02	3.57	0.72	1.78	1.51	1.09	0.22	2.81	0.28	0.11	0.02
	TS	55.11	4.72	0.76	0.08	17.08	1.26	5.98	0.76	0.08	0.04	3.36	0.64	1.54	0.83	0.91	0.30	2.83	0.30	0.10	0.02
Bk	SB	41.25	5.09	0.57	0.08	12.69	1.22	5.68	1.30	0.14	0.04	3.68	0.76	14.10	3.50	0.68	0.18	2.17	0.23	0.10	0.02
	TS	39.77	4.43	0.54	0.08	11.74	1.16	4.81	0.83	0.11	0.03	3.85	0.68	16.49	3.79	0.86	0.73	2.03	0.29	0.10	0.02
Cr		48.71	2.49	0.67	0.05	14.01	1.16	5.92	0.82	0.10	0.04	3.94	0.83	8.59	2.22	0.78	0.13	2.57	0.20	0.11	0.01

Horizon	Surface	LOI (%)	±	Ba (mg/kg)	±	Ce (mg/kg)	±	Co (mg/kg)	±	Cr (mg/kg)	±	Cu (mg/kg)	±	Ga (mg/kg)	±	La (mg/kg)	±	Nb (mg/kg)	±	Ni (mg/kg)	±
A	SB	11.15	6.97	444.54	47.60	80.83	13.19	20.23	5.93	134.04	17.78	38.48	6.53	17.90	4.89	45.38	11.52	15.07	2.91	77.50	12.01
	TS	12.26	3.67	424.72	41.79	85.74	18.31	23.80	8.44	148.49	32.42	41.10	16.96	20.39	5.06	44.48	9.81	17.09	2.43	85.70	14.64
Bk	SB	18.93	3.21	310.56	40.12	58.86	11.15	17.92	6.25	114.11	17.66	35.73	7.73	14.13	4.76	30.20	9.12	11.32	3.06	64.64	6.47
	TS	19.68	2.99	298.73	49.05	55.49	13.50	14.06	5.13	111.34	14.88	31.84	6.70	15.00	3.99	29.93	7.27	12.73	2.48	63.94	6.12
Cr		14.59	1.49	336.55	35.41	59.59	8.67	18.47	4.89	138.11	43.87	39.23	6.89	17.80	1.72	32.68	5.28	14.10	0.92	98.25	41.55

Horizon	Surface	Pb (mg/kg)	±	Rb (mg/kg)	±	S (mg/kg)	±	Sc (mg/kg)	±	Sr (mg/kg)	±	V (mg/kg)	±	Y (mg/kg)	±	Zn (mg/kg)	±	Zr (mg/kg)	±
A	SB	21.03	3.34	136.57	16.29	712.19	1010.04	13.08	4.29	154.32	30.51	121.06	16.62	31.30	3.95	105.66	12.60	194.08	32.00
	TS	21.78	2.89	156.08	18.74	773.26	712.82	15.81	5.81	147.64	22.62	135.84	31.60	33.31	4.61	107.89	15.38	194.16	48.24
Bk	SB	15.19	2.38	89.28	14.24	243.46	164.81	14.63	5.53	342.63	152.41	103.70	15.66	22.23	4.21	83.37	11.77	107.56	22.55
	TS	14.18	3.09	93.54	15.11	520.84	609.23	14.01	6.40	332.30	74.79	93.44	16.58	23.29	3.04	77.58	9.50	121.42	30.09
Cr		17.48	2.34	110.72	17.38	172.73	103.66	13.62	4.18	267.82	53.87	105.51	12.99	25.91	1.85	86.52	8.76	129.54	24.91

Horizon	Surface	$(CaO+MgO)/Al_2O_3$	±	$(CaO+MgO+K_2O+Na_2O)/Al_2O_3$	±	Ba/Sr	±	Rb/Sr	±	Al_2O_3/SiO_2	±	Al_2O_3/TiO_2	±
A	SB	0.33	0.12	0.56	0.12	3.00	0.75	0.91	0.17	0.29	0.02	22.17	2.17
	TS	0.29	0.08	0.51	0.09	2.93	0.45	1.08	0.19	0.31	0.04	22.85	2.91
Bk	SB	1.44	0.48	1.67	0.48	1.05	0.45	0.30	0.09	0.31	0.03	22.43	2.21
	TS	1.77	0.48	2.02	0.49	0.96	0.35	0.30	0.09	0.30	0.03	21.85	2.18
Cr		0.91	0.20	1.15	0.21	1.32	0.35	0.44	0.16	0.29	0.02	21.04	1.53

Table 2. Summary statistics and major- and trace-element indices for paleosols 'TS' and 'SB' (A and Bk horizons) and for unaltered floodplain parent material (Cr horizon). For quantitative primary data, see Supplementary Table 2.

Key element ratios were calculated (Table 2) along selected paleosol profiles (Fig. 5) and plotted in binary diagrams (Fig. 6). Table 2 permits a comparison of average values for selected geochemical parameters along the study paleosols. Six geochemical indices are reported below as a function of depth.

6.1. Calcification index

The $(CaO+MgO)/Al_2O_3$ ratio (calcification index) is a general proxy for pedogenic carbonate (calcite and dolomite) accumulations (Retallack, 2001a, b; 2007; Mohanty and Nanda, 2016). Generally, calcification is associated with processes that occur in dry climates where evaporation exceeds precipitation (Delgado et al., 2019).

In the study samples, the calcification index clearly discriminates between low values in A horizons and moderate values in Bk horizons, with no overlap (Fig. 5, Table 2). CaO is strongly depleted in upper A horizons (average values: 1.78% at the SB, 1.54% at the TS), whereas it is significantly enriched in Bk horizons (average values: 14.10% in SB paleosols, 16.49% in TS paleosols). Unaltered floodplain deposits exhibit intermediate values (8.59%). On the other hand, MgO values are fairly constant across distinct paleosol horizons and very similar to unweathered floodplain silts and clays (Table 2). Calculated $(CaO+MgO)/Al_2O_3$ ratios for A horizons are all fairly low, average values ranging between 0.29 (TS paleosols) and 0.33 (SB paleosols). On the other hand, average values for Bk horizons are in the 1.44 (SB paleosols) – 1.77 (TS paleosols) range and denote marked calcification. The calcification index averages 0.91 in unaltered Cr horizons (Table 2).

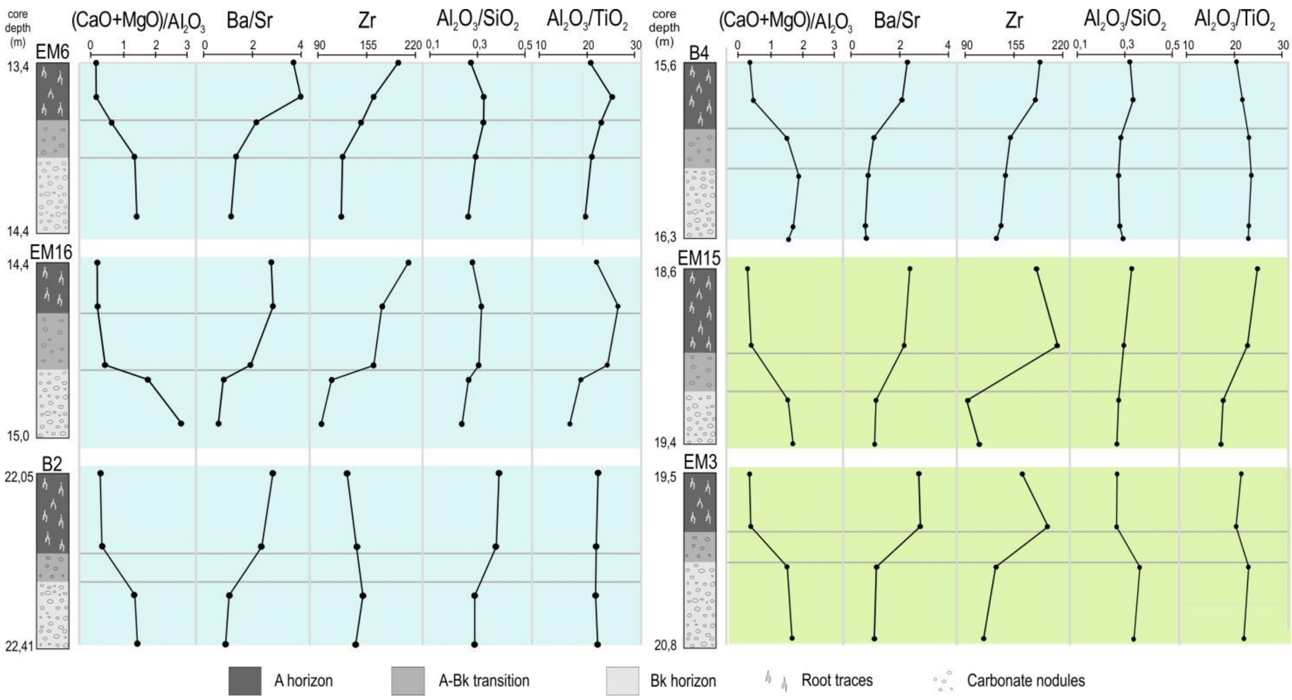

Fig. 5. Variations of major- and trace-element indices along selected paleosol profiles (see Figs. 3-4). TS paleosols (cores EM6, EM16, B2 and B4) are in light blue, SB paleosols (cores EM15 and EM3) in light green.

6.2. Base loss index

The ∑Bases/Al_2O_3 ratio, $(CaO+MgO+Na_2O+K_2O)/Al_2O_3$, measures the loss of mobile cations Ca^{2+}, Mg^{2+}, Na^+ and K^+, given as oxides, with respect to stable alumina (Ruxton, 1968; Mora and Driese, 1999; Retallack, 1999; Sheldon and Tabor, 2009). This index, which unlike the Chemical Index of Alteration (Nesbitt and Young, 1982) takes into account the role of Mg-bearing minerals, provides an indication of leaching of the bases from the soil system in response to weathering intensity (Retallack, 1999). The $(CaO+MgO+Na_2O+K_2O)/Al_2O_3$ index is similar to the Chemical Weathering Index (Harnois, 1988) and is the reciprocal of the hydrolysis ratio (Sheldon and Tabor, 2009). Chemical weathering affects plagioclase preferentially, then K-feldspar (Nesbitt et al., 1996). Calcium, sodium and potassium generally are removed from these minerals by aggressive soil solutions so that the proportion of alkalis to alumina typically decreases in the weathered product (Nesbitt and Young, 1982). In case of overwhelming weathering control, mobile elements are expected to be all depleted in surface horizons (He et al., 2020), whereas Bk horizons typically exhibit values higher than 1 (Dal' Bó et al., 2009).

In Po Plain paleosols, horizons A and Bk are clearly differentiated through the ∑Bases/Al_2O_3 ratio (Fig. 6a and Table 2), with notably similar results for older (SB) and younger (TS) paleosols. Average values for A horizons range between 0.51 (TS paleosols) and 0.56 (SB paleosols), whereas average values for Bk horizons are in the range of 1.67 (SB paleosols) – 2.02 (TS paleosols). This index has average value of 1.15 in Cr horizons (Table 2).

6.3. Leaching index

The Ba/Sr ratio quantifies the amount of leaching during the weathering process using the behaviour of alkaline earth metals like Ba and Sr (Retallack, 2001a, b; Sheldon and Tabor, 2009; Scarciglia et al., 2018). Although Ba and Sr have similar atomic radii and the same molecular affinity, Sr is more soluble than Ba (Vinogradov, 1959) and the Ba/Sr ratio increases with increasing weathering (Nesbitt and Young, 1982). Strontium dissolution in soils follows the same pathways as calcium. On the other hand, the chemical behaviour of Ba is less understood than Sr, particularly in soils (Sheldon and Tabor, 2009). The Rb/Sr ratio has been suggested as another indicator of the degree of weathering (Chen et al., 1999; Xu et al., 2010). Because the ionic radius of Rb is close to that of K, Rb generally coexists with K in K-rich minerals, such as K-feldspar and biotite, whereas Sr is preferentially partitioned into Na- and Ca-bearing minerals, such as carbonates, plagioclase and amphibole. Weathering can leach Ca and Sr much easier than Rb and K. As a result, the relict would have higher Rb/Sr ratios compared with the leached fraction. The Rb/Sr has also been used as a paleoclimatic indicator in loess-paleosol complexes (Chen et al., 1999).

The behaviour of the Ba/Sr leaching proxy mirrors that of the calcification index, allowing further differentiation between A and Bk horizons (Figs. 5 and 6b). Ba/Sr ratios for A horizons exhibit moderate average values that range between 2.93 (TS paleosols) and 3.00 (SB paleosols), whereas consistent, notably lower average values (0.96 for TS paleosols, 1.05 for SB paleosols) were obtained for Bk horizons. Unaltered floodplain material (Cr horizons) yielded an average value of 1.32 (Table 2). In the study paleosols, the Rb/Sr ratio behaves as the Ba/Sr ratio and decreases steadily downcore (Table 2). An obvious trend of Rb enrichment and Sr depletion is observed in A horizons (Fig. 5). Average values of the Rb/Sr ratio for A horizons range between

0.91 (SB paleosols) and 1.08 (TS paleosols), whereas for Bk horizons they are equal to 0.30. In the parent material (Cr horizon), the Rb/Sr ratio has an average value of 0.44 (Table 2).

6.4. Zr (zirconium)

Trace element geochemistry of paleosols provides valuable information regarding leaching and the degree of weathering (Retallack, 1999; 2001; Kahman et al., 2008; Mohanty and Nanda, 2016). Certain elements, such as Zr and Ti, are preferentially hosted in the densest minerals (e.g., zircon, ilmenite and monazite – Garzanti and Andò, 2019) and their concentration may vary owing to selective-entrainment effects (Garzanti et al., 2013; He et al., 2020). Zirconium (Zr), in particular, is commonly found in minerals that are resistant to alteration and therefore tends to accumulate as weathering progresses (Maynard, 1992; Mongrain et al., 2013; Driese et al., 2000), especially in the very fine sand-silt fraction (Garcia et al., 2003).

In the study paleosols, Zr shows a conspicuous decrease downprofile (Fig. 5 and Table 2), with few exceptions (e.g., core B2). An average value of 194 mg/kg is observed in A horizons, irrespective of paleosol age (SB vs TS), whereas significantly lower average values (108 mg/kg for SB paleosols, 121 mg/kg for TS paleosols) are recorded for Bk horizons. The average Zr concentration for unaltered Cr horizons is 130 mg/kg.

6.5. Clayeyness index

The Al_2O_3/SiO_2 ratio is a method for quantifying the amount of clay formation (Ruxton, 1968; Retallack et al., 2000; Prochnow et L., 2006), because Al accumulates in clay minerals relative to a silicate parent material (Sheldon and Tabor, 2009). Higher values are indicative of increasing clay formation with the loss of feldspars and other less resistant minerals (Ruxton, 1968; Sheldon and Tabor, 2009).

In the study samples, the clayeyness index contributes little geochemical signal, with minimal variations across the weathering profiles (Fig. 5), irrespective of paleosol horizons (A versus Bk) or ages (SB versus TS paleosols) (Table 2). For A horizons, average values of the Al_2O_3/SiO_2 ratio are narrowly constrained between 0.29 (SB paleosols) and 0.31 (TS paleosols). B horizons yielded very similar average values, ranging between 0.30 (TS) and 0.31 (SB). A similar clayeyness average value (0.29) was also obtained for the unweather floodplain material (Cr horizon in Table 2).

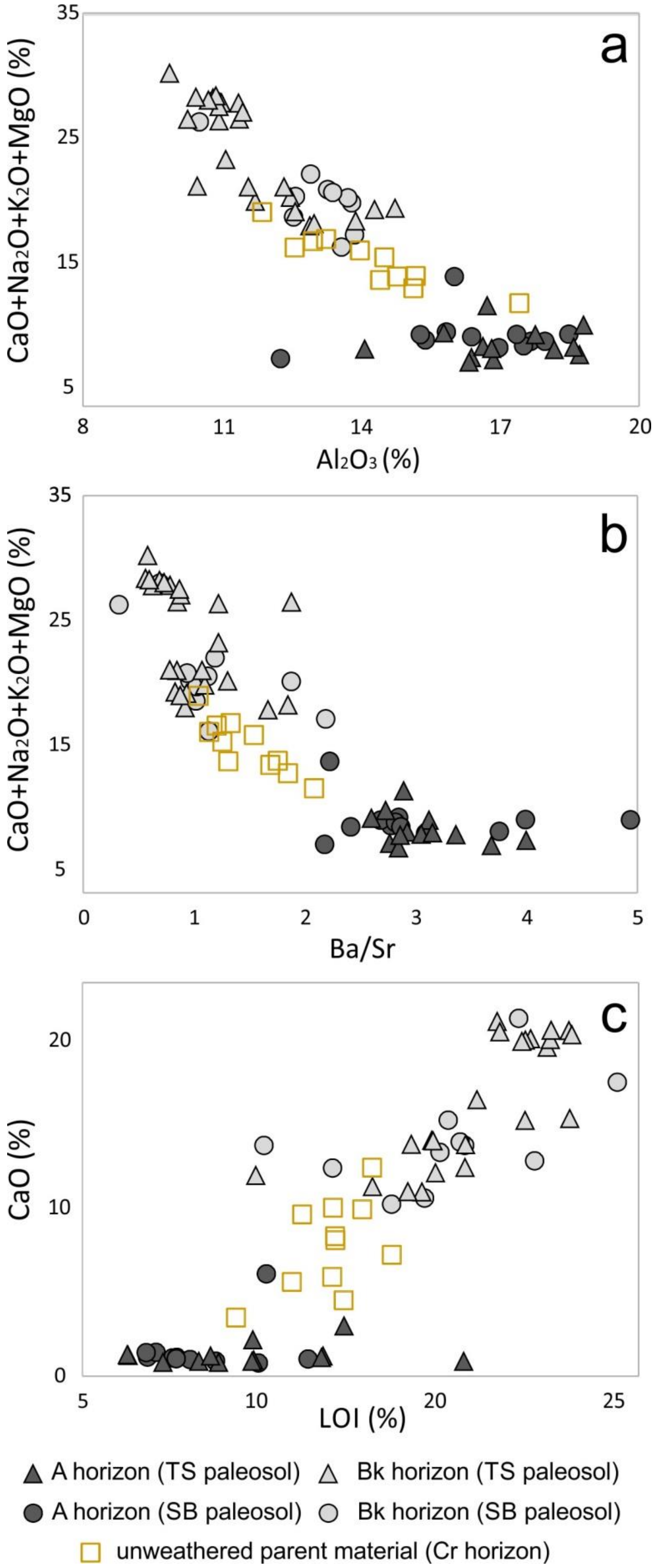

Fig. 6. Geochemical plots for 24 representative paleosols from 17 sediment cores (Fig. 1), grouped by horizon (A versus Bk) and sequence-stratigraphic position ('SB' versus 'TS' paleosols). Data are plotted against geochemical data from unweathered floodplain silts and clays (Cr horizon) from the same cores. a: Cross-plot of Al_2O_3 vs (CaO+MgO+Na_2O+K_2O); b: Cross-plot of Ba/Sr vs (CaO+MgO+Na_2O+K_2O); c: Cross-plot of LOI vs CaO.

6.6. Al_2O_3/TiO_2 ratio

This ratio is particularly useful as a provenance indicator, because Ti contents may be quite variable among different types of rocks, even as Al contents are relatively constant (Sheldon and Tabor, 2009). As both Al and Ti are relatively immobile elements, their ratio generally remains constant during pedogenesis (Delgado et al., 2019).

Average ratios of Al_2O_3/TiO_2 exhibit little variation at different profile localities and are fairly uniform across the various paleosol profiles, with no significant distinction between A horizons (22.17 for SB paleosols, 22.85 for TS paleosols) and Bk horizons (21.85 for TS paleosols, 22.43 for SB paleosols). This implies relatively homogeneous provenance.

The major geochemical variations shown along six paleosol profiles (Fig. 5) are consistent with data from 24 paleosols and 17 sediment cores (Fig. 6). In the ∑Bases/Al_2O_3 cross-plot (Fig. 6a), data points from the A horizons, Bk horizons and the unaltered parent material reveal a strong negative correlation and plot in three distinct clusters, irrespective of the key sequence-stratigraphic surface (SB or TS) at which sampled were collected. Elemental analysis shows that Bk horizons invariably have the highest $CaO+MgO+Na_2O+K_2O$ values. Particularly, ∑Bases yielded higher values in Bk horizons than in A horizons by an average factor 3.5 (Table 2). Data from the unaltered parent material invariably fall between these two extremes (Fig. 6a).

The roughly linear pattern of the ∑Bases versus Al_2O_3 plot is also seen with some trace elements, like Ba/Sr (Fig. 6b), and with LOI (Fig. 6c), that behave as CaO. Figures 6b and 6c reveal that there is a systematic trend in geochemical element distribution, with higher Sr concentrations and LOI values being prevalent in Bk horizons. At the other extreme, A horizons exhibit the lowest values in all paleosols.

7. Paleosol maturity

As Upper Pleistocene Po Plain paleosols underwent very incipient diagenesis, they still preserve most of their morphological and physico-chemical properties and environmental signatures. In general, paleosols are partitioned into two major pedogenic layers or horizons (Figs. 4-6). Basic identification features of paleosols include differences in color from darker A horizons to underlying lighter Bk horizons that reflect organic matter inputs in A horizons and calcium carbonate accumulation in Bk horizons (Schwertmann, 1993).

The relative rates of formation and characteristic stages of morphologies of Bk horizons have been quantified by Gile et al. (1965, 1966), Machette (1985) and Retallack (1988) for modern soils and Quaternary paleosols. According to such classification schemes, the presence of few to common carbonate nodules in calcareous (Bk) horizons allows attribution of Po Plain paleosols to Stage II of carbonate accumulation (Machette, 1985) and to the second stage of paleosol development (weakly developed paleosols of Retallack, 1988), which in fine-grained materials imply a few thousands of years to form (Birkeland, 1999). The rates of carbonate dissolution and reprecipitation in Bk horizons have been modelled by McFadden and Tinsley (1985) and mathematical models are available to estimate carbonate accumulation in soils (Mc Fadden et al., 1991; 1998). These studies are consistent with radiometric dating of Po Plain Inceptisols from the Bologna area, which also concluded that substantial pedogenic carbonate horizons formed during intervals of time of a few thousand years (Amorosi et al., 2014a; Bruno et al., 2020). Dominance of pedogenic carbonates in calcic horizons and weak pedogenic development suggest relatively dry conditions and the presence of a vadose zone and low groundwater table (Demko et al., 2004; Srivastava et al., 2018; Bruno et al., 2020). The presence of calcareous paleosols at the sequence boundary and on lowstand surfaces suggests that pedogenesis took place during times of relative climatic aridity and possibly reduced precipitation (Tandon and Gibling, 1997; Sinha et al., 2007).

Examination of geochemistry of Quaternary paleosols yields quantitative estimates of paleosol maturity and shows that paleosols bracketing the SB or developed at the landward equivalent of the TS have nearly uniform chemistry and display broadly similar stages of development throughout both dip-oriented (Fig. 3a) and strike-oriented (Fig. 3b) cross-sections. On homogeneous parent material, such as in the case of Quaternary Po Plain floodplain deposits, weathering indices change systematically with depth (Price and Velbel, 2003). Accordingly, geochemical variations in element ratios are observed at discrete levels within the study paleosols, allowing the clear differentiation between A and Bk horizons.

Pedogenesis may increase the relative amount of alumina in sediments. Nearly constant Al_2O_3/SiO_2 values with depth observed in Po Plain paleosols (Fig. 5 and Table 2) suggest that no significant clay illuviation took place in deeper horizons. This is consistent with the lack of well developed argillic (Bt) horizons along the paleosol profiles. Calculated values of the Al_2O_3/SiO_2 ratio are consistent with field observations and indicate that there is little textural variation throughout paleosol profiles. They also indicate that pedogenesis occurred on homogeneous silt- and clay-rich floodplain facies (Sprague et al., 2009).

Degradation of feldspars and other minerals by the removal of base cations (mostly Ca) by dissolution and concomitant formation of clay minerals is the dominant process during chemical weathering of silicate rocks (Nesbitt and Young, 1982). Mobile elements hosted in A horizons undergo extensive leaching and are progressively subtracted from feldspars. Leaching of mobile components (including CaO and MgO) is associated with enrichment of immobile elements, such as Zr (Fig. 5 and Table 2).

All geochemical proxies behave consistently. Selected indices that are commonly inferred to quantify the totality of weathering processes, such as calcification and Ba/Sr (Fig. 5 and Table 2) coherently reflect low degree of weathering under relatively cold climate conditions. It is apparent that several geochemical elements follow distinct patterns of geochemical variability and that downcore geochemical trends from all the study cores are consistent along paleosol profiles and represent pedochemical markers on a basin scale (Delgado et al., 2019). The most notable down-profile variation is increased concentration of labile oxides (CaO and MgO) with respect to Al_2O_3. Such negative Ca translocations from A horizons to underlying Bk horizons largely reflect weathering and removal of this labile cation relative to stable residual constituents. Base cations were leached from upper soil horizons in response to acidification processes and rapidly accumulated within the calcareous subsoil, reflecting the accumulation of pedogenic carbonate. Elevated LOI values in Bk horizons, paralleled by CaO levels (Fig. 6c), are interpreted to reflect the liberation of CO_2 during ignition of samples due to abundant carbonate (Cleveland et al., 2008). LOI data were then not considered further in interpretation.

Table 2 outlines the geochemical elements evaluated in this study and provides a comparison of the six element ratios plotted in Figs. 5 and 6. Significant leaching of the parent material to form paleosols is also inferred from the Ba/Sr and Rb/Sr ratios, which increase from Bk to A horizons. The enriched values of these “leaching parameters” in the A horizons are interpreted to reflect Sr removal from A horizons and accumulation of Sr-rich carbonate nodules in Bk horizons in association with Ca. Sequestration of Sr in the pedogenic carbonate phases and substitution of Sr for Ca are likely phenomena in the paleosol profile (Driese et al., 2000).

Concentrations of redox-sensitive trace elements, such as Cu, V, Cr, Ni, Co and Zn are notably higher in A horizons (Table 2). For the other trace elements, Zr is typically enriched in A horizons (Fig. 5). The abundance of Zr can be controlled by multiple geological factors other than weathering, including parent-rock material, grain size and hydraulic sorting (He et al., 2020). In the study area, perceptible enrichment in Zr concentration within A horizons is interpreted to reflect weathering: prolonged stability of interfluve surfaces is suggested by concentration of resistant heavy-minerals, such as zircons, in A horizons (Driese et al., 2000; Mongrain et al., 2013).

8. Use of immature paleosols for regional correlations

Weakly-developed paleosols represent regional surfaces of non-deposition that play a critical role in the high-resolution stratigraphy of the Upper Pleistocene, non-marine succession of the Po Plain. Pedogenic alteration is ubiquitous across the weathered interfluve surfaces and paleosols in key stratigraphic positions bear unique and consistent physico-chemical characteristics that can be effective in delineating subsurface stratigraphy of low-accommodation (FSST+LST) fluvial deposits on a regional scale (Figs. 2 and 3). Radiocarbon dating of SB and TS paleosols provides values consistent with radiocarbon ages observed from their updip equivalents, in the Bologna region (Amorosi et al., 2014a; Bruno et al., 2020). The remarkably similar stratigraphic architecture of Upper Pleistocene alluvial deposits in the study area (Fig. 3) with respect to regional paleosol stratigraphy (Fig. 2) suggests a similar history of deposition and pedogenesis that was likely produced under relatively cold climate conditions (LGM and YD, respectively) in response to allogenic controlling factors.

McCarthy and Plint (2013) have shown that paleosols characteristics at key sequence-stratigraphic surfaces may vary on a basin scale depending upon their paleo-landscape position with respect to valley margins and the marine shoreline, and that they can be partitioned into three distinct spatial zones based on their degree of development and architecture. The study area (Fig. 1) represents a relatively short segment of the wider Po Plain-Adriatic Sea source-to-sink system and displays no remarkable lateral variability in terms of physiographic location (Fig. 2). Within this relatively homogeneous alluvial plain segment, paleosol maturity does not exhibit significant differences in terms of pedogenic features (Fig. 4) and geochemical properties (Figs. 5-6). Poor lateral geochemical variability of paleosol characteristics on a km-scale has also been documented by Driese and Ashley (2016) and by Hyland and Sheldon (2016).

Further updip, at a greater distance from the margin of the Po paleovalley system, Late Pleistocene interfluve surfaces experienced higher intensities of pedogenic processes owing to their more elevated paleo-landscape position. At these locations, the immature paleosols (Inceptisols) described from the subsurface of the Po Plain are replaced by an intensely rubified Alfisol characterized by strong clay illuviation (Cremaschi, 1987; Cremaschi et al., 1990). This soil crops out continuously at the Apennines foothills and documents through a catenary effect a remarkably higher degree of soil development than in the buried distal units (Cremaschi and Nicosia, 2012). For a detailed documentation of alternating phases of sediment aggradation, stabilization and pedogenesis at the Apennines margin during the Late Pleistocene, the reader is referred to Zuffetti et al. (2018).

Subsurface control may predict the approximate position of SB and TS paleosols across the Po Basin fill through integration of physical stratigraphy with radiometric data (Figs. 3 and 4). This study has shown that framing precisely paleosol location into three-dimensional analysis can be largely aided by intrinsic geochemical properties (Figs. 5 and 6). Paleosol TS, developed at the Pleistocene/Holocene boundary, is readily recognized by its diagnostic stratigraphic position below Holocene transgressive deposits (Fig. 3). On the other hand, immature paleosols capped by the SB may stack one on another in a welded fashion as accommodation lessens (Figs. 2 and 4). For such paleosols, especially if no radiocarbon dates are available, correlation of soil-forming intervals bracketing the sequence boundary can be more useful than is attempting to correlate individual paleosols (McCarthy and Plint, 2013).

Extracting the weathering signal from geochemical data is not straightforward, as: (i) bulk sediment analysis cannot differentiate precisely among the several possible sources of each element (He et al., 2020); (ii) weathering indices might represent the integrated weathering history in the river basin, rather than being reliable proxies of instantaneous chemical weathering (Shao and Yang, 2012); (iii) the geochemistry of sediments can be affected by multiple controls other than climate-induced weathering, including source-rock lithology (Kraus, 2002) and hydraulic sorting (Garzanti and Resentini, 2016).

A careful evaluation of these diverse controls on sediment composition is possible in the study area and this can facilitate interpretation of weathering indices as reflecting true weathering indicators. For example, it is apparent that changes in source-rock lithology did not play a major role in controlling geochemical signatures of Upper Pleistocene paleosols. Sediment provenance analysis in the Po Plain based on integrated sand petrography (Tentori et al., 2021) and bulk-sediment geochemistry (Amorosi et al., 2012, 2014b; Amorosi and Sammartino, 2018; Bruno et al., 2017b) has shown that overbank parent material reflects a relatively homogeneous (Apennines) source-rock domain for Pleistocene alluvial deposits, as opposed to a remarkably more complex sediment dispersal pattern developed at the onset of the Holocene (Amorosi and Sammartino, 2018). Size sorting during transportation and deposition generally results in some degree of mineralogical differentiation, which may modify weathering indices (Garzanti and Resentini, 2016). Restricting paleosol composition to uniform mud grades, as also indicated by remarkably constant Al_2O_3/SiO_2 ratios (Table 2), makes the influence of grain size on composition minimal (Nesbitt and Young, 1982). Therefore, the composition of muds will primarily reflect the degree of weathering.

In summary, weathered horizons of Late Pleistocene age bear distinctive geochemical properties that are laterally traceable for tens of kilometers (Figs. 5 and 6) and that can be used as highly effective stratigraphic markers across the non-marine portion of the Po Basin fill. They also represent the key to unravel the sequence-stratigraphic architecture of the non-marine succession, tracing systems tract boundaries from the downstream segments of the source-to-sink system into the upstream alluvium.

9. Conclusions

Two weakly developed paleosols marking the sequence boundary (SB) and the lateral equivalent of the transgressive surface (TS), respectively, in the Last Glacial Maximum depositional sequence are laterally continuous and traceable for tens of kilometers across the non-marine portion of the Po Basin. Such surfaces provide a comprehensive, three-dimensional view of the pedogenic character of Late Pleistocene interfluves. This paper has investigated the modifications induced by chemical weathering on such pedogenically altered floodplain deposits, focusing on the recognition, correlation, and characterization of Inceptisol-like paleosols.

A comparison of the paleosols, their distribution, and degree of pedogenic development suggest widespread soil development on short-lived, interfluvial areas. Weakly developed paleosols mark regional unconformities and contain excellent records of the Late Pleistocene depositional history. They are linked to minimal incision and their alternation with overbank deposits into paleosol-bearing cycles reflects conditions of limited accommodation on the floodplain and their formation as a result of alternate aggradation and degradation. The most distinctive feature of SB and TS paleosols is soil partitioning into a well identifiable dark, organic-matter-rich and carbonate-free upper A horizon and a lower Bk horizon, typified by the abundance of calcium carbonate nodules.

Weathering patterns, expressed as geochemical trends, of paleosols represent discernible regional features that define a robust correlation scheme, with small lateral variability and suggest that floodplain environments were affected by mild, but laterally extensive weathering conditions. Element ratios used as tracers of the degree of weathering (calcification and base loss indices) represent pedochemical markers that do not show substantial modifications along strike and dip, and that exhibit consistent behaviour with depth across paleosol profiles. Translocation of Ca, with almost complete removal from the upper portions and concentration in lower horizons is a diagnostic feature of Po Plain paleosols. Some trace metal ratios experience significant variations across the weathering zones. Ba/Sr and Rb/Sr typically show a loss in the A horizons and gain in the Bk horizons, which is consistent with the identification of calcic horizons. On the other hand, redox-sensitive trace elements and Zr show increasing values from the parent material to upper paleosol horizons.

Acknowledgments

We are indebted to two anonymous reviewers, Guest Editors Giorgio Basilici and Augusto Varela, and Editor-in-Chief Thomas Algeo for their valuable and constructive comments and suggestions.

References

Aitken, J.F., Flint, S.S., 1996. Variable expressions of interfluvial sequence boundaries in the Breathitt Group (Pennsylvanian), eastern Kentucky, USA. Geological Society, London, Special Publications 104, 193–206.

Amorosi, A., Sammartino, I., 2018. Shifts in sediment provenance across a hierarchy of bounding surfaces: A sequence-stratigraphic perspective from bulk-sediment geochemistry. Sedimentary Geology 375, 145–156.

Amorosi, A., Centineo, M.C., Dinelli, E., Lucchini, F., Tateo, F., 2002. Geochemical and mineralogical variations as indicators of provenance changes in Late Quaternary deposits of SE Po Plain. Sedimentary Geology 151, 273–292.

Amorosi, A., Bruno, L., Rossi, V., Severi, P., Hajdas, I., 2014a. Paleosol architecture of a late Quaternary basin--margin sequence and its implications for high-resolution, non-marine sequence stratigraphy. Global and Planetary Change 112, 12–25.

Amorosi, A., Guermandi, M., Marchi, N., Sammartino, I., 2014b. Fingerprinting sedimentary and soil units by their natural metal contents: a new approach to assess metal contamination. Science of the total environment 500, 361–372.

Amorosi, A., Bruno, L., Campo, B., Morelli, A., 2015. The value of pocket penetration tests for the high-resolution palaeosol stratigraphy of late Quaternary deposits. Geological Journal 50, 670–682.

Amorosi, A., Bruno, L., Campo, B., Morelli, A., Rossi, V., Scarponi, D., Hong, W., Bohacs, K.M., Drexler, T.M., 2017a. Global sea-level control on local parasequence architecture from the Holocene record of the Po Plain, Italy. Marine and Petroleum Geology 87, 99–111.

Amorosi, A., Bruno, L., Cleveland, D.M., Morelli, A., Hong, W., 2017b. Paleosols and associated channel-belt sand bodies from a continuously subsiding late Quaternary system (Po Basin, Italy): New insights into continental sequence stratigraphy. Bulletin 129, 449–463.

Amorosi, A., Bruno, L., Campo, B., Costagli, B., Hong, W., Picotti, V., Vaiani, S.C., 2020. Deformation patterns of upper Quaternary strata and their relation to active tectonics, Po Basin, Italy. Sedimentology.

Anderson, J.B., Rodriguez, A., Abdulah, K.C., Fillon, R.H., Banfield L.A., McKeown, H.A., Wellner, J.S., 2004. Late Quaternary stratigraphic evolution of the northern Gulf of Mexico Margin: A synthesis. In: Anderson, J.B., Fillon, R.H. (Eds.), Late Quaternary Stratigraphic Evolution of the Northern Gulf of Mexico Margin. Society for Sedimentary Geology, Special Publication 79, 1–23.

Atchley, S.C., Nordt, L.C., Dworkin, S.I., 2004. Eustatic control on alluvial sequence stratigraphy: a possible example from the Cretaceous-Tertiary transition of the Tornillo Basin, Big Bend National Park, West Texas, USA. Journal of Sedimentary Research 74, 391–404.

Autin, W.J., Aslan, A., 2001. Alluvial pedogenesis in Pleistocene and Holocene Mississippi River deposits: Effects of relative sea-level change. Geological Society of America Bulletin 113, 1456–1466.

Bersezio, R., Giudici, M., Mele, M., 2007. Combining sedimentological and geophysical data for high-resolution 3-D mapping of fluvial architectural elements in the Quaternary Po Plain (Italy). Sedimentary Geology 202, 230–248.

Birkeland, P.W., 1999. Soils and Geomorphology, (3rd Ed.). Oxford University Press, New York. 448 pp.

Blum, M.D., Price, D.M., 1998. Quaternary alluvial plain construction in response to glacio-eustatic and climatic controls, Texas Gulf coastal plain. In: Shanley, K.W., McCabe, P.W. (Eds.), Relative Role of Eustasy, Climate, and Tectonism in Continental Rocks: SEPM Special Publication 59, 31–48.

Blum, M.D., Aslan, A., 2006. Signatures of climate vs. sea-level change within incised valley-fill successions: Quaternary examples from the Texas Gulf coast. Sedimentary Geology 190, 177–211.

Bruno, L., Amorosi, A., Severi, P., Costagli, B., 2017a. Late Quaternary aggradation rates and stratigraphic architecture of the southern Po Plain, Italy. Basin Research 29, 234–248.

Bruno, L., Bohacs, K.M., Campo, B., Drexler, T.M., Rossi, V., Sammartino, I., Scarponi, D., Hong, W., Amorosi, A., 2017b. Early Holocene transgressive palaeogeography in the Po coastal plain (northern Italy). Sedimentology 64, 1792–1816.

Bruno, L., Piccin, A., Sammartino, I., Amorosi, A., 2018. Decoupled geomorphic and sedimentary response of Po River and its Alpine tributaries during the last glacial/post-glacial episode. Geomorphology 317, 184–198.

Bruno, L., Campo, B., Di Martino, A., Hong, W., Amorosi, A., 2019. Peat layer accumulation and post-burial deformation during the mid-late Holocene in the Po coastal plain (Northern Italy). Basin Research 31, 621–639.

Bruno, L., Marchi, M., Bertolini, I., Gottardi, G., Amorosi, A., 2020. Climate control on stacked paleosols in the Pleistocene of the Po Basin (northern Italy). Journal of Quaternary Science 35, 559–571.

Busschers, F.S., Kasse, C., van Balen, R.T., Vandenberghe, J., Cohen, K.M., Weerts, H.J.T., Wallinga, J., Johns, C., Cleveringa, P., Bunnik, F.P.M., 2007. Late Pleistocene evolution of the Rhine–Meuse system in the southern North Sea basin: imprints of climate change, sea-level oscillation, and glacio-isostacy. Quaternary Science Reviews 26, 3216–3248.

Campo, B., Amorosi, A., Vaiani, S.C., 2017. Sequence stratigraphy and late Quaternary paleoenvironmental evolution of the Northern Adriatic coastal plain (Italy). Palaeogeography, Palaeoclimatology, Palaeoecology 466, 265–278.

Campo, B., Bohacs, K.M., Amorosi, A., 2020. Late Quaternary sequence stratigraphy as a tool for groundwater exploration: Lessons from the Po River Basin (northern Italy). American Association of Petroleum Geologists Bulletin 104, 681–710.

Castiglioni, G.B., 2001. Response of the fluvial system to environmental variations. In: Castiglioni, G.B., Pellegrini, G.B. (Eds.), Illustrative Notes of the Geomorphological Map of Po Plain (Italy). Geografia Fisica Dinamica Quaternaria 4, 165–188.

Chen, J., An, Z., Head, J., 1999. Variation of Rb/Sr ratios in the loess-paleosol sequences of Central China during the last 130,000 years and their implicationsfor monsoon paleoclimatology. Quaternary Research 51, 215–219.

Chen, Q., Li, C., Li, P., Liu, B., Sun, H., 2008. Late Quaternary paleosols in the Yangtze Delta, China, and their paleoenvironmental implications. Geomorphology 100, 465–483.

Choi, K., Kim, J.H., 2006. Identifying late Quaternary coastal deposits in Kyonggi Bay, Korea, by their geotechnical properties. Geo-Marine Letters 26, 77–89.

Cleveland, D.M., Atchley, S.C., Nordt, L.C., 2007. Continental sequence stratigraphy of the Upper Triassic (Norian--Rhaetian) Chinle strata, northern New Mexico, USA: allocyclic and autocyclic origins of paleosol-bearing alluvial successions. Journal of Sedimentary Research 77, 909–924.

Cleveland, D.M., Nordt, L.C., Atchley, S.C., 2008. Paleosols, trace fossils, and precipitation estimates of the uppermost Triassic strata in northern New Mexico. Palaeogeography, Palaeoclimatology, Palaeoecology 257, 421–444.

Cremaschi, M., 1987. Paleosols and Vetusols in the Central Po Plain (Northern Italy): a study in Quaternary geology and soil development. Unicopli, Milan. 306 p.

Cremaschi, M., Nicosia, C., 2012. Sub-Boreal aggradation along the Apennine margine of the Central Po Plain: geomorphological and geoarchaeological aspects. Géomorphologie: relief, processus, environnement 2, 155–174.

Cremaschi, M., Fedoroff, N., Guerreschi, A., Huxtable, J., Colombi, N., Castelletti, L., Maspero, A., 1990. Sedimentary and pedological processes in the upper Pleistocene loess of Northern Italy. The Bagaggera sequence. Quaternary International 5, 23–38.

Dabrio, C.J., Zazo, C., Goy, J.L., Sierro, F.J., Borja, F., Lario, J., González, J.A., Flores, J.A., 2000. Depositional history of estuarine infill during the last postglacial transgression (Gulf of Cadiz, Southern Spain): Marine Geology 162, 381–404.

Dal' Bó, P.F., Basilici, G., Angelica, R.S., Bernardes Ladeira, F.S., 2009. Paleoclimatic interpretations from pedogenic calcretes in a Maastrichtian semi-arid eolian sand-sheet palaeoenvironment: Marília Formation (Bauru Basin, southeastern Brazil). Cretaceous Research 30, 659–675.

Delgado, L., Batezelli, A., Ladeira, F.S.B., Luna, J. 2019. Paleoenvironmental and paleoclimatic interpretation of the Late Cretaceous Marília Formation (Brazil) based on paleosol geochemistry. Catena 180, 365–382.

Demko, T.M., Currie, B.S., Nicoll, K.A., 2004. Regional paleoclimatic and stratigraphic implications of paleosols and fluvial/overbank architecture in the Morrison Formation (Upper Jurassic), Western Interior, USA. Sedimentary Geology 167, 115–135.

Driese, S.G., Ashley, G.M., 2016. Paleoenvironmental reconstruction of a paleosol catena, the Zinj archaeological level, Olduvai Gorge, Tanzania. Quaternary Research 85, 133–146.

Driese, S.G., Mora, C.I., Stiles, C.A., Joeckel, R.M., Nordt, L.C., 2000. Mass-balance reconstruction of a modern Vertisol: implications for interpreting the geochemistry and burial alteration of paleo-Vertisols. Geoderma 95, 179–204.

Fan, D., Shang., S., Burr, G., 2019. Sea level implications from late Quaternary/Holocene paleosols from the Oujiang delta, China. Radiocarbon 61, 83–99.

Franzini, M., Leoni, L., Saitta, M., 1972. A simple method to evaluate the matrix effects in X-ray fluorescence analysis. X-ray Spectrometry 1, 151–154.

Garcia, D., Joseph, P., Maréchal, B., Moutte, J., 2003. Patterns of geochemical variability in relation to turbidite facies in the Grès d'Annot Formation. In: P. Joseph, S.A. Lomas, Deep-Water Sedimentation in the Alpine Basin of SE France: New Perspectives on the Grès d'Annot and related systems. Geological Society London, Special Publications 221, 349–365.

Garzanti, E., Resentini, A., 2016. Provenance control on chemical indices of weathering (Taiwan river sands). Sedimentary Geology 336, 81–95.

Garzanti, E., Andò, S., 2019. Heavy minerals for junior woodchucks. Minerals 9, 148.

Garzanti, E., Padoan, M., Andò, S., Resentini, A., Vezzoli, G., Lustrino, M., 2013. Weathering and relative durability of detrital minerals in equatorial climate: sand petrology and geochemistry in the East African Rift. The Journal of Geology 121, 547–580.

Gibling, M.R., Bird, D.J., 1994. Late Carboniferous cyclothems and alluvial paleovalleys in the Sydney Basin, Nova Scotia: The Geological Society of America Bulletin 106, 105–117.

Gibling, M.R., Fielding, C.R., Sinha, R., Davidson, S.K., Leleu, S., North, C.P., 2011. Alluvial valleys and alluvial sequences: towards a geomorphic assessment. From River to Rock Record: The Preservation of Fluvial Sediments and Their Subsequent Interpretation: SEPM, Special Publication 97, 423–447.

Gile, L.H., Peterson, F.F., Grossman, R.B., 1965. The K horizon: a master soil horizon of carbonate accumulation. Soil Science 99, 74–82.

Gile, L.H., Peterson, F.F., Grossman, R.B., 1966. Morphological and genetic sequences of carbonate accumulation in desert soils. Soil Science 101, 347–360.

Harnois, L., 1988. The CIW index: a new chemical index of weathering. SedG 55, 319–322.

He, J., Garzanti, E., Dinis, P., Yang, S., Wang, H., 2020. Provenance versus weathering control on sediment composition in tropical monsoonal climate (South China) – 1. Geochemistry and clay mineralogy. Chemical Geology 558, 119860.

Hyland, E.G., Sheldon, N.D., 2016. Examining the spatial consistency of palaeosol proxies: Implications for palaeoclimatic and palaeoenvironmental reconstructions in terrestrial sedimentary basins. Sedimentology 63, 959–971.

Janssens, M.M., Kasse, C., Bohncke, S.J.P., Greaves, H., Cohen, K.M., Wallinga, J., Hoek, W.Z., 2012. Climate-driven fluvial development and valley abandonment at the last glacial-interglacial transition (Oude IJssel-Rhine, Germany). Netherlands Journal of Geosciences 91, 37–62.

Kahmann, J.A., Driese, S.G., 2008. Paleopedology and geochemistry of Late Mississippian (Chesterian) Pennington Formation paleosols at Pound Gap, Kentucky, USA: Implications for high-frequency climate variations. Palaeogeography, Palaeoclimatology, Palaeoecology 259, 357–381.

Kasse, C., Bohncke, S.J.P., Vandenberghe, J., Gábris, G., 2010. Fluvial style changes during the last glacial–interglacial transition in the middle Tisza valley (Hungary): Proceedings of the Geologists' Association 121, 180–194.

Kraus, M.J., 2002. Basin-scale changes in floodplain paleosols: implications for interpreting alluvial architecture. Journal of Sedimentary Research 72, 500–509.

Kvale, E.P., Archer, A.W., 2007. Paleovalley fills: Trunk vs. tributary. American Association of Petroleum Geologists Bulletin 91, 809–821.

Leoni, L., Saitta, M., 1976. Determination of yttrium and niobium on standard silicate rocks by X-ray fluorescence analyses. X-ray Spectrometry 5, 29–30.

Leoni, L., Menichini, M., Saitta, M., 1982. Determination of S, Cl and F in silicate rocks by X-Ray fluorescence analyses. X-Ray Spectrometry 11, 156–158.

Machette, M.N., 1985. Calcific soils of the southwestern United States. Soils and Quaternary geology of the southwestern United States: Geological Society of America Special Paper 203, 1–21.

Marriott, S.B., Wright, V.P., 1993. Palaeosols as indicators of geomorphic stability in two Old Red

Sandstone alluvial suites, South Wales. Journal of the Geological Society 150, 1109–1120.

Maynard, J.B., 1992. Chemistry of modern soils as a guide to interpreting Precambrian paleosols. The Journal of Geology 100, 279–289.

McCarthy, P.J., Plint, A.G., 1998. Recognition of interfluve sequence boundaries: integrating paleopedology and sequence stratigraphy. Geology 26, 387–390.

McCarthy, P.J., Plint, A.G., 2003. Spatial variability of palaeosols across Cretaceous interfluves in the Dunvegan Formation, NE British Columbia, Canada: palaeohydrological, palaeogeomorphological and stratigraphic implications. Sedimentology 50, 1187–1220.

McCarthy, P.J., Plint, A.G., 2013. A pedostratigraphic approach to nonmarine sequence stratigraphy: a three-dimensional paleosol-landscape model from the Cretaceous (Cenomanian) Dunvegan Formation, Alberta and British Columbia, Canada. In: Driese, S.G., Nordt, L.C. (Eds.), New Frontiers in Paleopedology and Terrestrial Paleoclimatology: Paleosols and Soil Surface Analog Systems: Society for Sedimentary Geology Special Publication 104, 159–177.

McFadden, L.D., Tinsley, J.C., 1985. Rate and depth of pedogenic-carbonate accumulation in soils: formulation and testing of a compartment model, in: Soils and Quaternary Geology of the Southwestern United States. Geological Society of America, pp. 23–41.

McFadden, L.D., Amundson, R.G., Chadwick, O.A., 1991. Numerical Modeling Chemical, and Isotopic Studies of Carbonate Accumulation in of Arid Regions. Occurrence, characteristics, and genesis of carbonate, gypsum, and silica accumulations in soils 26, 17–35.

McFadden, L.D., McDonald, E. V, Wells, S.G., Anderson, K., Quade, J., Forman, S.L., 1998. The vesicular layer and carbonate collars of desert soils and pavements: formation, age and relation to climate change. Geomorphology 24, 101–145.

Mohanty, S.P., Nanda, S., 2016. Geochemistry of a paleosol horizon at the base of the Sausar Group, central India: Implications on atmospheric conditions at the Archean--Paleoproterozoic boundary. Geoscience Frontiers 7, 759–773.

Mol, J., 1997. Fluvial response to Weichselian climate changes in the Niederlausitz (Germany). Journal of Quaternary Science: Published for the Quaternary Research Association 12, 43–60.

Mongrain, J.R., McCarthy, P.J., Plint, A.G., Fowell, S.J., 2013. Integrated paleopedology and palynology from alluvial paleosols of the Cretaceous (Cenomanian) Dunvegan Formation, Alberta and British Columbia, Canada: paleoenvironmental and stratigraphic implications. In: Driese, S.G., Nordt, L.C. (Eds.), New Frontiers in Paleopedology and Terrestrial Paleoclimatology: Paleosols and Soil Surface Analog Systems: Society for Sedimentary Geology Special Publication 104, 231–255.

Mora, C.I. and Driese, S.G., 1999. Paleoenvironment, paleoclimate and stable carbon isotopes of Paleozoic red-beds palaeosols, Appalachian Basin, U.S.A. and Canada. In: Thiry, M. and Coincon, R.S. (Eds.), Palaeoweathering, Palaeosurfaces, and Related Continental Deposits: International Association of Sedimentologists, Special Publication 27, 61–84.

Morelli, A., Bruno, L., Cleveland, D.M., Drexler, T.M., Amorosi, A., 2017. Reconstructing Last Glacial Maximum and Younger Dryas paleolandscapes through subsurface paleosol stratigraphy: An example from the Po coastal plain, Italy. Geomorphology 295, 790–800.

Nesbitt, H.W., Young, G.M., 1982. Early Proterozoic climates and plate motions inferred from major element chemistry of lutites. nature 299, 715–717.

Nesbitt, H.W., Young, G.M., McLennan, S.M., Keays, R.R., 1996. Effects of chemical weathering and sorting on the petrogenesis of siliciclastic sediments, with implications for provenance studies. The Journal of Geology 104, 525–542.

Plint, A.G., McCarthy, P.J., Faccini, U.F., 2001. Nonmarine sequence stratigraphy: updip expression of sequence boundaries and systems tracts in a high-resolution framework, Cenomanian Dunvegan Formation, Alberta foreland basin, Canada. AAPG bulletin 85, 1967–2001.

Price, J.R., Velbel, M.A., 2003. Chemical weathering indices applied to weathering profiles developed on heterogeneous felsic metamorphic parent rocks. Chemical Geology 202, 397–416.

Prochnow, S.J., Nordt, L.C., Atchley, S.C., Hudec, M.R., 2006. Multi-proxy paleosol evidence for middle and late Triassic climate trends in eastern Utah. Palaeogeography, Palaeoclimatology, Palaeoecology 232, 53–72.

Reigemborn, M.S., Beilinson, E., 2020. Stratigraphic architecture and paleosols as basin correlation tools of the early Paleogene infill in central–south Patagonia, Golfo San Jorge Basin, Argentinean Patagonia. J. S. Am. Earth Sci. 99, 102519.

Retallack, G.J., 1988. Field Recognition of Paleosols. GSA Sp. Paper, pp. 1–20.

Retallack, G.J., 1997a. Early forest soils and their role in Devonian global change. Science 276, 583–585.

Retallack, G.J., 1997b. Neogene expansion of the North American prairie. Palaios 12, 380–390.

Retallack, G.J., 1997c. Palaeosols in the upper Narrabeen Group of New South Wales as evidence of Early Triassic palaeoenvironments without modern analogues. Australian Journal of Earth Sciences 44, 185–201.

Retallack, G.J., 1999. Post-apocalyptic greenhouse paleoclimate revealed by earliest Triassic paleosols in the Sydney Basin, Australia. Geological Society of America Bulletin 111, 52–70.

Retallack, G.J., 2001a. Soils of the Past: an Introduction to Paleopedology, 2nd Rev., Blackwell Publishing, Oxford. 404 p.

Retallack, G.J., 2001b. Cenozoic expansion of grasslands and climatic cooling. The Journal of Geology 109, 407–426.

Retallack, G.J., 2007. Soils and global change in the carbon cycle over geological time. In: Holland, H.D., Turekian, K.K. (Eds.), Treatise on geochemistry, v. 5. Pergamon Press, Oxford, pp. 581–605.

Retallack, G.J., Bestland, E.A., Fremd, T., 2000. Eocene and Oligocene paleosols and environmental change in central Oregon. Geological Society of America Special Paper 344, 192 pp.

Ruxton, B.P., 1968. Measures of the degree of chemical weathering of rocks. The Journal of Geology 76, 518–527.

Shanley, K.W., McCabe, P.J., 1994. Perspectives on the sequence stratigraphy of continental strata. American Association of Petroleum Geologists Bulletin 78, 544–568.

Shao, J.Q., Yang, S.Y., 2012. Does chemical index of alteration (CIA) reflect silicate weathering and monsoonal climate in the Changjiang River basin? Chinese Science Bulletin 57, 1178–1187.

Scarciglia, F., Mercatante, G., Fondevilla, V., Anadón, P., Oms, O., Donato, P., Agnini, C., Papini, M., Rook, L., Ghinassi, M., 2018. Pleistocene paleosol development and paleoenvironmental dynamics in Easr Africa: A multiproxy record from the Homo-bearing Aalat pedostratigraphic succession, Dandiero basin (Eritrea). Quaternary Science Reviews 191, 275–298.

Schwertmann, U., 1993. Relations between iron oxides, soil color, and soil formation. Soil color 31, 51–69.

Sheldon, N.D., Tabor, N.J., 2009. Quantitative paleoenvironmental and paleoclimatic reconstruction using paleosols. Earth-Science Reviews 95, 1–52.

Sinha, R., Kumar, R., Sinha, S., Tandon, S.K., Gibling, M.R., 2007. Late Cenozoic fluvial successions in northern and western India: an overview and synthesis. Quaternary Science Reviews 26, 2801–2822.

Soil Survey Staff., 1999. Soil Taxonomy. A basic system of soil classification for making and interpreting soil surveys, Agricultural Handbook. Natural Resources Conservation Service, USDA: Washington, DC. 436.

Sprague, R.A., Melvin, J.A., Conradi, F.G., Pearce, T.J., Dix, M.A., Hill, S.D., Canham, H., 2009. Integration of core-based chemostratigraphy and petrography of the Devonian jauf sandstones. In: Uthmaniya Area, Ghawar Field, Eastern Saudi Arabia. AAPG Search and Discovery Article 20065, pp. 34.

Srivastava, P., Rajak, M.K., Sinha, R., Pal, D.K., Bhattacharyya, T., 2010, A high-resolution micromorphological record of the Late Quaternary paleosols from Ganga-Yamuna interfluve: stratigraphic and paleoclimatic implications: Quaternary International, v. 227, no. 2, p. 127–142.

Srivastava, P., Sinha, R., Deep, V., Singh, A., Upreti, N., 2018. Micromorphology and sequence stratigraphy of the interfluve paleosols from the Ganga Plains: a record of alluvial cyclicity and paleoclimate during the Late Quaternary. Journal of Sedimentary Research 88, 105–128.

Tandon, S.K., Gibling, M.R., 1997. Calcretes at sequence boundaries in Upper Carboniferous cyclothems of the Sydney Basin, Atlantic Canada. Sedimentary Geology 112, 43–67.

Tentori, D., Amorosi, A., Milli, S., Marsaglia, K.M., 2021. Sediment dispersal pathways in the Po coastal plain since the Last Glacial Maximum: provenance signals of autogenic and eustatic forcing. Basin Research 33, 1407–1428.

van Balen, R.T., Busschers, F.S., Tucker, G.E., 2010. Modeling the response of the Rhine--Meuse fluvial system to Late Pleistocene climate change. Geomorphology 114, 440–452.

Van Wagoner, J.C., Mitchum, R.M., Campion, K.M., Rahmanian, V.D., 1990. Siliciclastic sequence stratigraphy in well logs, cores, and outcrops: concepts for high-resolution correlation of time and facies. American Association of Petroleum Geologists, Methods in Exploration 7: Tulsa, U.S.A, 55 p.

Varela, A.N., Raigemborn, M.S., Richiano, S., White, T., Poiré, D.G. Lizzoli, S., 2018. Late Cretaceous paleosols as paleoclimate proxies of high-latitude Southern Hemisphere: Mata Amarilla Formation, Patagonia, Argentina. Sedimentary Geology 363, 83–95.

Vinogradov, A.P., 1959. Geochemistry of isotopes. International Geology Review 1, 1–13.

Xu, Z., Liu, C.-Q., 2010. Water geochemistry of the Xijiang basin rivers, South China: Chemical weathering and CO2 consumption. Applied Geochemistry 25, 1603–1614.

Zuffetti, C., Trombino, L., Zembo, I., Bersezio, R., 2018. Soil evolution and origin of landscape in a late Quaternary tectonically mobile setting: The Po Plain-Northern Apennines setting in Lombardy (Italy). Catena 171, 376–397.

Supplementary Table 1. Location and elevation of the 17 cores studied for geochemical analysis.

Supplementary Table 2. XRF geochemistry (major and trace element analysis) of the study paleosols.